# Single-Molecule Imaging of L-Type Ca$^{2+}$ Channels in Live Cells

Gregory S. Harms,* Laurent Cognet,* Piet H. M. Lommerse,*† Gerhard A. Blab,* Heike Kahr,‡
Roland Gamsjäger,‡ Herman P. Spaink,† Nikolai M. Soldatov,§ Christoph Romanin,‡ and Thomas Schmidt*

Departments of *Biophysics and †Biology, Leiden University, 2333 CA Leiden, The Netherlands, ‡Institute for Biophysics, University of Linz, 4040 Linz, Austria, and §National Institute on Aging, National Institutes of Health, Baltimore, Maryland 21224, USA

ABSTRACT   L-type Ca$^{2+}$ channels are an important means by which a cell regulates the Ca$^{2+}$ influx into the cytosol on electrical stimulation. Their structure and dynamics in the plasma membrane, including their molecular mobility and aggregation, is of key interest for the in-depth understanding of their function. Construction of a fluorescent variant by fusion of the yellow-fluorescent protein to the ion channel and expression in a human cell line allowed us to address its dynamic embedding in the membrane at the level of individual channels in vivo. We report on the observation of individual fluorescence-labeled human cardiac L-type Ca$^{2+}$ channels using wide-field fluorescence microscopy in living cells. Our fluorescence and electrophysiological data indicate that L-type Ca$^{2+}$ channels tend to form larger aggregates which are mobile in the plasma membrane.

## INTRODUCTION

Single-molecule fluorescence imaging reveals great details about dynamical processes of biological interest in a multitude of in vitro systems (Weiss, 1999; Ishii and Yanagida, 2000; Edman et al., 1996; Dickson et al., 1997; Sase et al., 1997; Lu et al., 1998; Jia et al., 1999; van Oijen et al., 1999). This novel methodology, however, lacks a general utilization in vivo (Sako et al., 2000; Schütz et al., 2000), primarily because of the enhanced fluorescence background caused by the cellular autofluorescence and the lack of suitable fluorescence tags to label proteins in living cells. Fluorescent proteins provide a noninvasive and convenient means for the in vivo labeling of molecular components (Tsien, 1998). In the current study, we use a method which permits wide-field, single-molecule imaging of eYFP (enhanced yellow-fluorescent protein) fusion-proteins in living cells not masked by cellular autofluorescence.

The target of the current investigation is the cardiac L-type Ca$^{2+}$ channel, one of the major subjects in molecular cardiology and research in Ca$^{2+}$ signaling (Murphy et al., 1991; Fabiato and Fabiato, 1997; Rios and Brum, 1987; Gao et al., 1999). The channel protein consists of a pore-forming $\alpha_{1C}$-subunit and two auxiliary subunits (Hofmann et al., 1994; Catterall, 1995) (Fig. 1). Although a vast amount of functional information about this channel is available from electrophysiology (Catterall, 1995), our knowledge about its dynamic embedding in the cell membrane and its aggregation state in vivo is minute. Aggregation (Flucher and Fran-

zini-Armstrong, 1996; Grabner et al., 1998; Flucher et al., 1993) has been previously anticipated from well ordered arrays of the Ca$^{2+}$-release channels on membranes of the sarcoplasmic reticulum (Saito et al., 1988), which are closely coupled to the L-type Ca$^{2+}$ channels on the plasma membrane (Flucher and Franzini-Armstrong, 1996). In this study, we performed a detailed analysis of the fluorescence intensity in both position and time for functionally active individual eYFP-$\alpha_{1C}$ fusion protein molecules in the plasma membrane of the HEK293 cell line. This allowed us to obtain information about their mobility and the state of molecular aggregation. Surprisingly, it seems that the aggregation of L-type Ca$^{2+}$ channels is probably independent from its association with other structures of the excitation-contraction machinery (Gerster et al., 1999). The latter finding further confirms results obtained by electrophysiology (Kepplinger et al., 2000), and by in vitro studies of the purified channel when reconstituted in a phospholipid monolayer (Hinterdorfer et al., 1997).
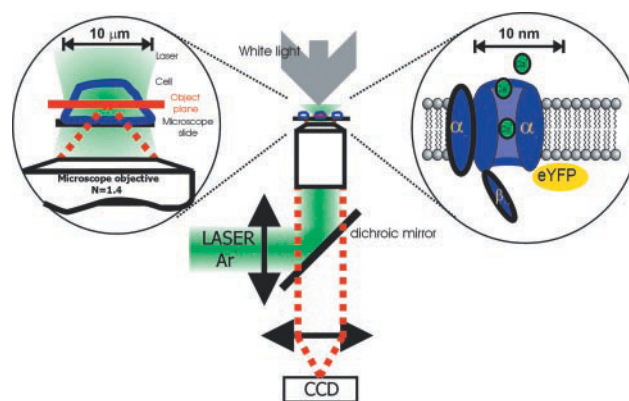
FIGURE 1   Diagram of the experimental setup (*center*). Signals of an entire cell localized in the object plane (*left inset*) are imaged on the CCD. The object plane is adjustable throughout the cell. Schematic structure of a L-type Ca$^{2+}$ channel in the membrane.

## MATERIALS AND METHODS

### Cloning of eYFP-$\alpha_{1C,77}$

Cloning and electrophysiological characterization of eYFP-$\alpha_{1C,77A}$ has been described in detail in Kepplinger et al. (2000). In brief, the 5′-terminal *Hind* III linker upstream Kozak sequence and 3′-terminal *Bgl* II linker were incorporated into the flanking regions of the peYFP DNA (Clontech Laboratories, Palo Alto, CA) open reading frame by polymerase chain reaction (PCR) using 5′-cttaagcttcgccaccatggtgagc-3′ sense and 5′-ag-atctcttgtacagctcgtcc-3′ antisense primers, respectively. The *Hind* III/*Bgl* II peYFP cassette was ligated with the *BamH I/Not* I HFCC77 cassette into the DNA3 vector (Invitrogen, Carlsbad, CA) at *Hind* III/*Not* I sites so that the eYFP-77pcDNA3 construct encoded the eYFP fused to $\alpha_{1C,77}$ via RSAT tetrapeptide. Integrity of the ORF was verified by sequencing.

### Cell culture

HEK293 cells were cultured in DMEM medium supplemented with strep-tomycin (100 $\mu$g/ml), penicillin (100 U/ml), and 10% bovine serum in a humidified atmosphere (95%) at 5% $CO_2$ and 37°C. Cells were used for 12–14 passages and were transferred every 4 days. Transfection was performed using N-[2,3-dioleoyloxy)propyl]-N,N,N-trimethylammonium methylsulfate (Amersham, Rosendaal, The Netherlands). Cells exhibiting confluence of ~30% were used for transfection with a total of, respec-tively, 0.25 (low transfection) and 2 $\mu$g (normal transfection) of cDNA (molar ratio of $\alpha_{1C,77}$-eYFP/$\beta_{2A}$ = 1/1.6 and $\alpha_{1C,77}$-eYFP/$\alpha_2/\delta$ = 1/1.4) in a 1-ml volume. The excess with $\beta_{2A}$ and $\alpha_2/\delta$ subunits assured a complete assembly of all $\alpha_{1C,77}$-eYFP units to a functional channel. This was concluded from the homogeneous behavior observed in the electrophysi-ological results in all patch-clamp trials. The transfection efficiency was in the range of 20–60%. For fluorescence measurement the cells were plated on #1 glass slides (Fisher, Zoetermeer, The Netherlands) in a bath of phosphate-buffered saline (150 mM NaCl, 10 mM $Na_2HPO_4$, pH 7.4).

### Electrophysiology

Details on the electrophysiological experiments, including the single chan-nel recording and analysis referred to later in this article, can be found in Kepplinger et al. (2000). Whole-cell patch-clamp recordings (Hamill et al., 1981) were obtained from HEK293 cells transfected with either $\alpha_{1C,77}$ or YFP-$\alpha_{1C,77}$ together with $\beta_{2A}$ and $\alpha_2/\delta$ subunits using an Axopatch 2B (Axon Instruments, Foster City, CA) or an EPC7 (Heka Elektronik, Lam-brecht, Germany) amplifier. The pipette solution contained: 120 mM Cs methane sulfonate, 5 mM $CaCl_2$, 2 mM $MgCl_2$, 10 mM HEPES, 10 mM EGTA, 2 mM MgATP, pH (CsOH) 7.3. The bath solution consisted of: 154 mM N-methyl glucamine, 1 mM $MgCl_2$, 5 mM D-glucose monohydrate, 10 mM HEPES, 5 mM 4-aminopyridine, 15 mM $BaCl_2$, pH (HCl) 7.4. Soft glass pipettes (Microhematocrit tubes, No. 564, Fa. Assistant, Vienna, Austria) with a resistance of 1–4 M$\Omega$ were used for whole-cell recordings. $Ba^{2+}$ currents were activated by repetitive (0.2 Hz) depolarizations from a holding potential of −80 mV to test potentials (0.244 s) between −10 mV and +60 mV with an incremental increase of 5 mV or 20 mV. Current traces were filtered at 3 kHz, digitized at 8 kHz, and were neither capacity nor leak current corrected allowing to verify the quality of voltage-clamp. A liquid junction potential of 6 mV was not taken into account. This value should be subtracted from all voltages in whole-cell recordings (Neher, 1992). All experiments were performed at room temperature.

### Single-molecule optical microscopy

The experimental arrangement for single-molecule imaging has been de-scribed in detail previously (Schmidt et al., 1995). Essentially, the samples were mounted onto an inverted microscope (Zeiss, Weesp, The Nether-
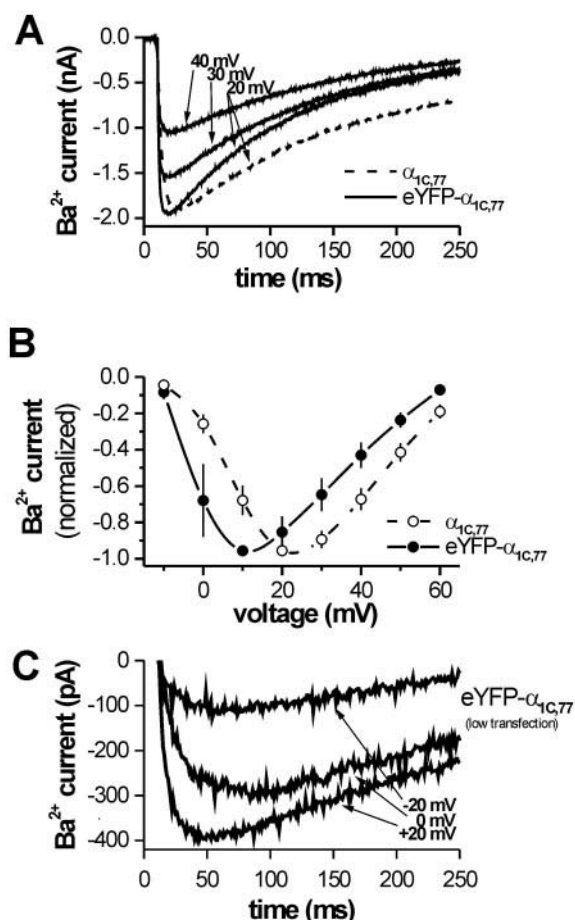


FIGURE 2  Electrophysiological characterization of the eYFP-$\alpha_{1C,77}$ fu-sion protein. (*A*) Comparison of whole cell $Ba^{2+}$ current of the wild-type L-type $Ca^{2+}$ channel with the eYFP-$\alpha_{1C,77}$ fusion protein. The cells were depolarized to +20, +30, and +40 mV from a holding potential of −80 mV. On average $I_{Ba}$ = 1690 ± 180 pA (mean ± SE, $N$ = 12) was observed on depolarization to +20 mV for the eYFP-$\alpha_{1C,77}$ channel. (*B*) Current-voltage characterization of the wild-type L-type $Ca^{2+}$ channel compared with the eYFP-$\alpha_{1C,77}$ fusion channel. (*C*) Whole-cell $Ba^{2+}$ current of the L-type $Ca^{2+}$ channel with the fusion of the eYFP on the $\alpha_{1C}$ subunit transfected with low concentration of plasmid in HEK cells. The cells were depolarized to −20, 0, and +20 mV from a holding potential of −80 mV. On average, $I_{Ba}$ was reduced to 200 ± 50 pA (mean ± SE, $N$ = 6).

lands) equipped with a 100× objective (NA = 1.4, Zeiss), and illuminated for 5–10 ms at 514 nm from an $Ar^+$-laser (Spectra Physics, Eindhoven, The Netherlands). The illumination intensity was set to 5 kW/cm$^2$ in all experiments. The excitation polarization was selected by a Berek polarizer (New Focus, San Jose, CA). Use of appropriate filter combinations (DCLP530, HQ580/75, Chroma Technology, Brattleboro, VT, and OG530–3, Schott, Mainz, Germany) permitted the detection of individual eYFPs by a nitrogen-cooled charge coupled device (CCD)-camera system (Princeton Instruments, Vianen, The Netherlands). The total detection efficiency of the experiment was 0.048.

For single-molecule detection cells were photobleached at 514 nm for typically 1 s at the intensity of 5 kW/cm$^2$. Fluorescence images were taken consecutively with a delay between 50 and 500 ms with up to a possible 500 images in a sequence. An analysis program determined the lateral position of each signal with an accuracy of <50 nm by fitting to a two-dimensional (2-D) Gaussian surface. The extremely high positional
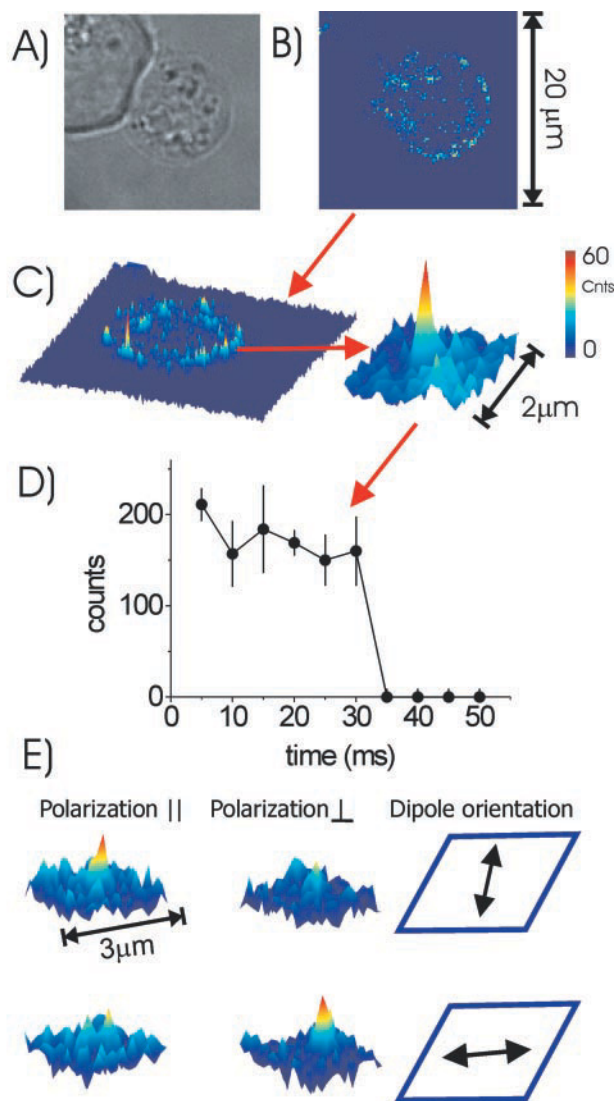
A Vogel-algorithm was used to correlate the images of molecules in subsequent observations from which the respective single-molecule trajectories were reconstructed (Schmidt et al., 1995). For each trajectory of length $N$ with respective positions

$$D_{lat} = [4\Delta t (N-1)]^{-1} \sum_i (\vec{p}_i - \vec{p}_{i-1})^2$$

and time-lag $\Delta t$, a mean diffusion constant (Sonnleitner et al., 1999) was evaluated by:

## Fluorescence correlation microscopy

Fluorescence correlation measurements were performed using a commercial system (ConfoCor, Zeiss). We used 514-nm excitation with standard optics, including a dichroic mirror (510 nm, Zeiss), a water-immersion objective (40×, 1.2 NA, Zeiss) and a band-pass filter (515–565 nm, Zeiss) to discriminate the fluorescence. The excitation intensity was <1 kW/cm² to reduce photobleaching of eYFP. The emission light was filtered by a 45-$\mu$m diameter pinhole, and detected by an avalanche photodiode connected to a fast digital correlator. Correlation curves were selected which exhibited correlation times significantly longer than the mean photobleaching time of ~50 ms. The correlation curves, $G(t)$, obtained for eYFP-$\alpha_{1C,77}$ in HEK293 cells were fit by the combination of 2-D diffusion and photobleaching (Schwille et al., 1999): $G(t) = N^{-1} (1 + t/t_d)^{-1} \exp(-t/t_b)$, where $t_d$ is the mean diffusion time, $t_b$ is the mean photobleaching time, and $N$ is the average number of fluorophores in the confocal volume. For diffusion analysis, only curves were accepted for which $t_b > 2 t_d$. Calibration of the size of the focused beam was performed with tetramethylrhodamine in water (Widengren and Rigler, 1998), yielding a beam radius of 0.32 $\mu$m. For display, all curves are normalized by multiplication with the mean number of fluorophores, $N$. The acquisition time was set to 10 s. Additional control experiments (not shown) were performed on purified eYFP in buffer solutions (including viscosity, pH, and salt effects) which confirmed the submillisecond timescale dynamics of eYFP reported in literature (Widengren et al., 1999; Schwille et al., 2000).

## RESULTS

### Single-molecule imaging

Fig. 1 depicts a schematic diagram of the experiments as described in Methods. Cardiac L-type Ca²⁺ channels consisting of the fluorescent N-terminally labeled subunit, eYFP-$\alpha_{1C,77}$, and the wild-type auxiliary subunits, $\beta_{2A}$ and $\alpha_2/\delta$, were expressed in HEK293 cells. Fluorescence images were taken from ~1-$\mu$m thick slices through the middle of the cells. It was apparent from those images (Figs. 3 *B* and 5 *A*) that most channels were translocated to the cell membrane.

To test for the functional integrity of the eYFP-$\alpha_{1C,77}$ fusion construct, an electrophysiological characterization was performed in parallel. We found (Fig. 2, *A* and *B*) that the N-terminal eYFP-fusion to the $\alpha_{1C,77}$ subunit did not significantly affect Ca²⁺ channel function in both whole-cell and single-channel experiments (Kepplinger et al., 2000). The channel inactivation was faster by ~30% and the activation curve was shifted by −10 mV with respect to the wild-type $\alpha_{1C,77}$ channel. These findings are in agree-

FIGURE 3 Single-molecule characterization. (*A*) White light and (*B*) fluorescence image of an HEK293 cell transfected with eYFP-$\alpha_{1C,77}$ subunits of a Ca²⁺ channel. (*C*) Enlarged fluorescence image. (*D*) The mean detected fluorescence attributable to an individual eYFP-$\alpha_{1C,77}$ is 34 cnts/ms. After 6 observations, a single-step photobleaching event occurred. (*E*) Polarization images taken at an interval of 110 ms showing a slow rotation of an individual eYFP-$\alpha_{1C,77}$ (the excitation light was circularly polarized). Only two images of a series are shown. It should be noted that such slow rotation was found for only 10% of all signals observed. The angles of the transition-dipole moment (*boxed arrows*) with respect to the laboratory coordinates were determined from the intensity ratio in the parallel ($\parallel$) and perpendicular ($\perp$) directions. All fluorescence images are scaled between 0 (*blue*) and 60 cnts/pxl (*red*).

accuracy obtained in single-molecule microscopy solely linked to the signal-to-background ratio, which was ~15 in the current experiments. The photon counts were determined with a precision of ~20%, limited by the shot-noise and readout-noise of the CCD-camera. It should be noted that because of the low coverage of the cell membrane with fluorescent proteins (<1 $\mu$m⁻²; separated point-emitters), the wide-field approach allows for axial separation of signals as seen in Fig. 3 *A*. The axial resolution in this case is characterized by the depth-of-focus of the microscope (~1 $\mu$m), which is notably smaller than the thickness of a cell (typically 5–10 $\mu$m).
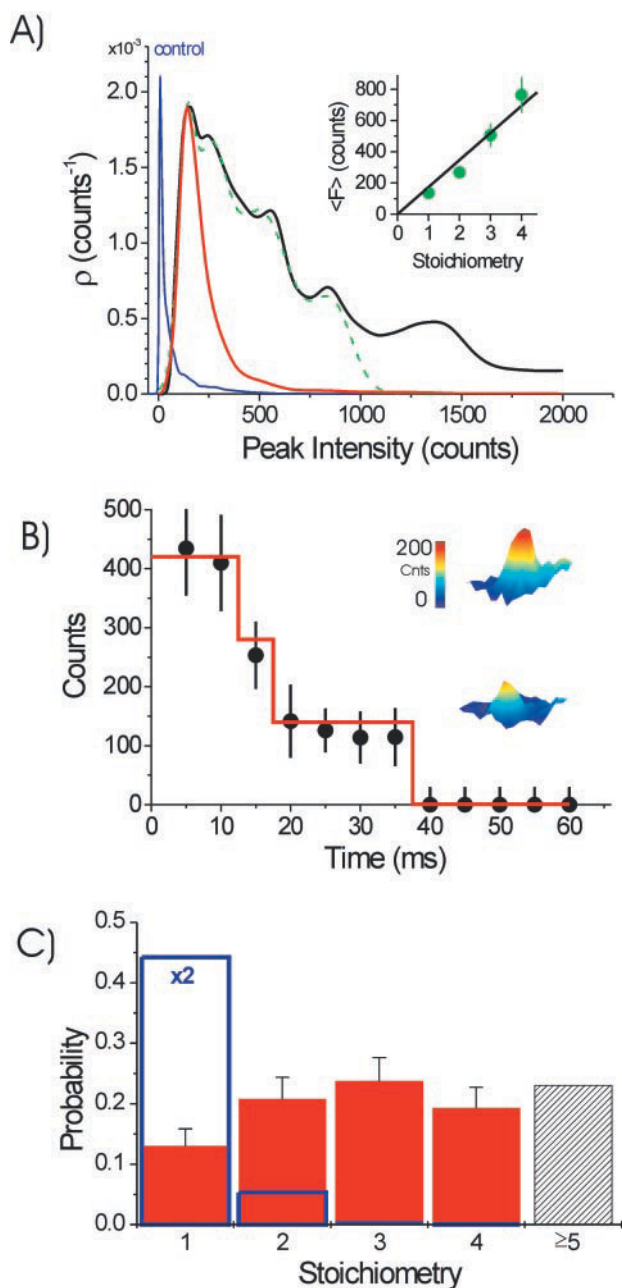
FIGURE 4  $Ca^{2+}$ channel clustering. (*A*) Probability density function, $\rho$, of the fluorescence signal constructed from 271 individual observations on the surface of an HEK293 cell. The distribution was fit for signal intensities <1000 cnts to 4 Gaussians (*dotted green line*). For comparison, the intensity distribution obtained from an untransfected cell ("control"), and the distribution from individual eYFP-his$_6$:Ni$^{2+}$-NTA chelated lipids in an artifical lipid membrane are shown (Harms et al., 2001) (*red curve*). The positions of the maxima in the distribution were equidistant with a slope of 168 cnts/5 ms (*inset*). (*B*) Intensity of individual signals as a function of time. For an eYFP-$\alpha_{1C,77}$ cluster a multiple-step (three-step) photobleaching event was observed. The horizontal lines are taken from the fit in Fig. 4 *A* inset. All fluorescence images are scaled between 0 (*blue*) and 200 cnts/pxl (*red*). (*C*) Statistical analysis of the stoichiometry of all 3417 observed signals (*solid column*). Assuming an even distribution of eYFP-$\alpha_{1C,77}$ with a density of 0.24 per resolution-limited area (0.08 $\mu m^2$), a Poisson distribution (*open columns*) is predicted.

ment with work on homologous proteins (Grabner et al., 1998; Gerster et al., 1999).

The single-molecule fluorescence results are conceptualized in Fig. 3. Images obtained by fluorescence microscopy easily discriminate cells that contained fluorescence-labeled channels from untransfected cells (compare Fig. 3 *A* and 3 *B*). Diffraction-limited fluorescence signals (320 ± 80 nm full-width at half-maximum) are localized at the cell surface and are distinguishable from the background with high signal-to-background-noise ratio (~15, Fig. 3 *C*). These localized signals fit well to 2-D Gaussian surfaces yielding values for the integrated fluorescence and the lateral position on the membrane. Subsequent positional tracking follows those signals over time at a rate of up to 20 images/s. Such detailed analysis allows us to assign the signals to individual eYFP-$\alpha_{1C,77}$ subunits of the L-type $Ca^{2+}$ channel. We find that the single fluorescent molecules have the following characteristics: (1) the mean amplitude of the smallest signal component of 34 ± 4 cnts/ms matches the mean amplitude found for individual eYFPs in buffer, 38 ± 4 cnts/ms, and mean signals found when eYFP is immobilized onto artificial- and cell-membranes, (36 ± 4 and 33 ± 4 cnts/ms, respectively), at identical illumination intensity and integration times (Harms et al., 2001). (2) All signals exhibited a stepwise photobleaching behavior (Fig. 3 *D*), a signature characteristic for a single-molecule event. (3) Fluorescence polarization imaging (Harms et al., 1999) (see Methods) shows that a fraction (<10%) of all signals exhibits fluorescence which is highly polarized. A high fluorescence polarization is a distinctive property for single quantum systems, such as a single fluorophore, if its rotation is slower than the detection time. The rotation of the fluorophore shown in Fig. 3 *E* results in a change of the direction of the transition dipole moment by 70 ± 20° in 110 ms. (4) Finally, fluorescence correlation experiments (Schwille et al., 1999; Widengren and Rigler, 1998) were performed from which the mean number of fluorescent entities was derived (~10 $\mu m^{-2}$). This independent finding further corroborates our results from single-molecule imaging (Fig. 5 *C*). These arguments together demonstrate, for the first time, observation of individual eYFP-fusion proteins in a living cell.

To achieve this result, we applied a rigorous experimental optimization. For the single-molecule imaging experiments, the transfection procedure is adjusted such that the number of channels per resolution limited area of 0.08 $\mu m^2$ was less than one. Fluorescence single-molecule measurements here require: (1) the reduction of the amount of plasmid by a factor of ~10 in comparison to transfection procedures normally applied in electrophysiology; (2) increasing the time between transfection and measurement to >4 days which additionally ensured a low cytosolic background; and (3) the selection of individual cells with low expression levels of the fusion protein (~$10^4$ copies per cell, corresponding to a surface density of ~30 $\mu m^{-2}$). Additionally,
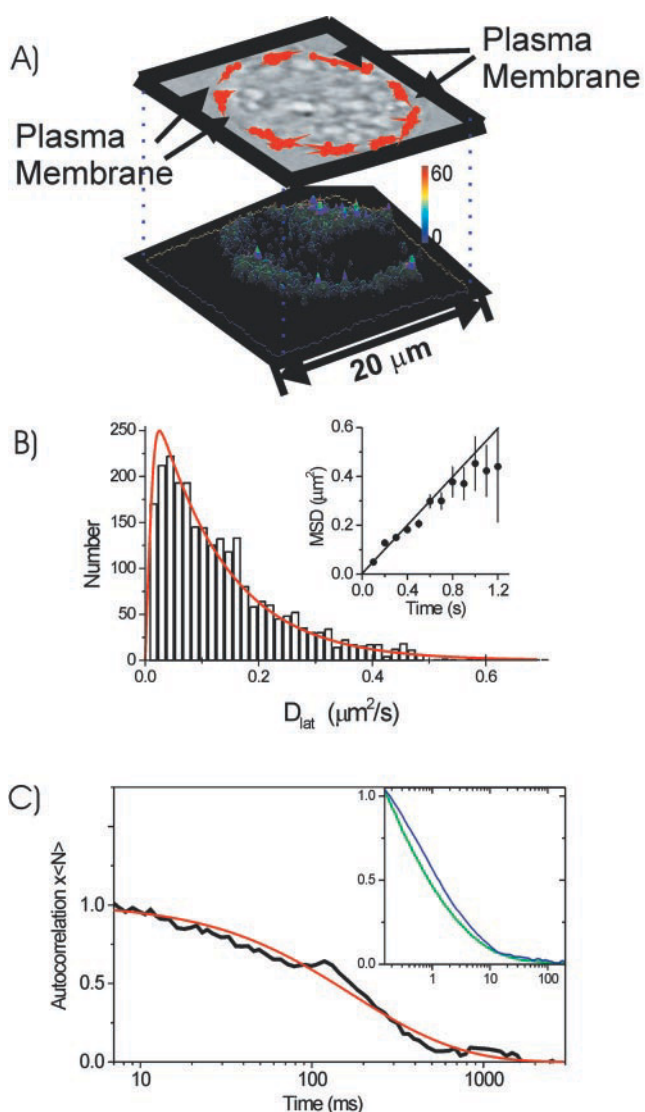
FIGURE 5   Ca$^{2+}$ channel mobility. (*A*) Ensemble of single-molecule trajectories (*red lines*) overlaid by a white-light image of an HEK293 cell. All trajectories are confined to the cell's perimeter. The fluorescence images are scaled between 0 (*blue*) and 60 cnts/pxl (*red*). (*B*) Distribution of lateral diffusion constants, $D_{lat}$, of 2492 individual eYFP-$\alpha_{1C,77}$ on the cell surface. The distribution has a mean of $D_{lat} = 0.15 \ \mu m^2/s$. For a linear analysis, a deviation from normal diffusion behavior does not occur up to a length scale of 0.7 $\mu m$ (*inset*). (*C*) Signal obtained by fluorescence correlation spectroscopy of eYFP-$\alpha_{1C,77}$ Ca$^{2+}$ channel subunits in HEK293 cells. Only correlation events longer than 50 ms were analyzed (see Methods). Fitting of the data to a 2-D diffusion model (*red curve*) yielded a diffusion time of 200 ms, which corresponds to a diffusion constant of 0.11 $\mu m^2/s$. Photobleaching events of a fraction of molecules between 50 and 600 ms likely account for the jaggedness of the correlation curve. *Inset*: Comparison with fluorescence correlation curves of nonfused eYFP in the cytosol of HEK293 cells (*blue*) and purified eYFP in phosphate-buffered saline (*green*).

photobleaching of the cells is necessary to reduce the autofluorescence to a basal level characterized by a value of 9.7 cnts/5 ms root-mean-square (see Fig. 4 *A* "control"). We

found that the photobleaching step also reduces the observable density of the eYFP-$\alpha_{1C,77}$ to $\sim$10% of the initial level leading to $\sim$3 observable eYFP-$\alpha_{1C,77}$ per $\mu m^2$. Together, the procedures permit reliable and reproducible single-molecule imaging and fluorescence correlation analysis of eYFP-$\alpha_{1C}$ with a high discrimination from cellular autofluorescence.

As an independent confirmation of our findings, the influence of the variation in the transfection procedures on the channel activity was investigated (Fig. 2 *C*). The electrophysiological experiments showed that under described conditions, the average peak Ba$^{2+}$ inward current was 200 $\pm$ 50 pA (mean $\pm$ SE, $N = 6$) at a depolarization to +20 mV, which is eight times less than the current recorded with the transfection procedures as used in Fig. 2, *A* and *B* (1690 $\pm$ 180 pA, $N = 12$). Given a single-channel conductivity of $\sigma = 29$ pS, the reverse potential of 63 mV (Fig. 2 *B*), and an open probability of $p_O = 0.03$ (Kepplinger et al., 2000), the average density of channels in a typical cell of diameter 10 $\mu m$ using the low transfection protocol is n $\sim$ 17 $\mu m^{-2}$ in registry with our estimations from the fluorescence. We have further tried to obtain single-channel recordings from cells which were transfected with the reduced amount of channel plasmid to determine a possible influence on the channel behavior. However, we were unable to obtain any single-channel recording in $N = 12$ trials.

## Ca$^{2+}$ channel clustering

Achievement of single-molecule sensitivity in fluorescence permits for a detailed analysis of local stoichiometries yielding information on channel aggregation. Fig. 4 *A* shows the fluorescence intensity distribution calculated from 271 individual fluorescence signals on the surface of an HEK293 cell. The distribution is far from unimodal, consisting of multiple central intensity values. This observation was confirmed to be characteristic for eYFP-$\alpha_{1C}$ expressed in HEK293 cells by comparison to the intensity distribution obtained for purified eYFP when anchored to a membrane (Harms et al., 2001). The intensity distribution of that control measurement was found to be close to a single Gaussian with a width mostly accounted for by the shot-noise and the instrument read-out noise of the CCD-camera. It should be noted, that the long timescale ($>$100 ms) "blinking" behavior of the autofluorescent proteins (Dickson et al., 1997; Schwille et al., 2000) could not be distinguished from diffusion in our experiments. The fast photophysical dynamics of the autofluorescent proteins observed on submillisecond timescales (Widengren et al., 1999; Schwille et al., 2000; Garcia-Parajo et al., 2000), are averaged out on the 5-ms illumination time used here, giving rise to a slightly larger widths of the intensity distributions compared with that of conventional fluorescence labels (Schmidt et al., 1996a).

For quantitative interpretation of the multimodal intensity distribution shown in Fig. 4 *A*, algorithms were used which have been described previously (Schmidt et al., 1996b). In brief, the lower part of the distributions (up to 1000 cnts) were first fit to four Gaussians for which the positions of the maxima were found to be equidistant with a spacing of $168 \pm 20$ cnts/5ms (Fig. 4 *A*, *inset*). It was also found that the squared widths of those Gaussians scaled linearly with the aggregation number as being predicted for statistically independent distributions. The spacing matches that of the mean intensity of an individual eYFP-$\alpha_{1C,77}$ ($34 \pm 4$ cnts/ms, Fig. 3 *D*), providing strong direct evidence for a local clustering of L-type $Ca^{2+}$ channels. Signal amplitudes >1000 cnts/5 ms were not taken into account for such detailed analysis. For those signals, the increased width of the Gaussian deems a reliable assignment unjustified (Schmidt et al., 1996b).

Subsequent to this global analysis, a more detailed analysis was applied for classification of each individual signal to a local stoichiometry (Schmidt et al., 1996b), $N$ ($N$ ranging from 1 to 4, and $\geq 5$) of detected eYFP-$\alpha_{1C,77}$; the intensity of the signal was compared with that obtained from individual eYFP protein molecules when anchored to a membrane (Fig. 4 *A*, *red curve*, and Harms et al., 2001). A priori knowledge of the monomer signal-distribution was used as a solid basis for our stoichiometry assignment. In total, 7 cells and 3417 signals were analyzed, yielding a probability of 0.13, 0.21, 0.24, 0.19, 0.23 for one, two, three, four, and more colocalized eYFP-$\alpha_{1C,77}$, respectively (Fig. 4 *C*). The distribution in Fig. 4 *C* is characterized by an average number of $3.1 \pm 0.3$ colocalized and detected eYFP-$\alpha_{1C,77}$ molecules. For determination of the overall size of the aggregates, the initial photobleaching step must be taken into account. Including photobleaching the observed distribution is given by a binomial characterized by the mean cluster size $M$ and the photobleaching probability, $1-P$. A least-squares fit yielded $M = 40 \pm 15$ and $P = 0.07 \pm 0.03$.

As the individual classification algorithm applied here is statistical (Schmidt et al., 1996b), it was occasionally confirmed by a direct method: for this the fluorescence intensity of individual signals was monitored over time. Some of the signals showed a one-step photobleaching behavior indicative for an individual eYFP-$\alpha_{1C,77}$ (Fig. 3 *D*), whereas others exhibited a multistep bleaching behavior (Fig. 4 *B*). Taken together with the equidistant fluorescence intensity distribution (Fig. 4 *A*, *inset*) from which the fluorescence levels for aggregates was predicted (*horizontal lines* in Fig. 4 *B*) those events were taken as a signature of multiple eYFP-$\alpha_{1C,77}$ bleaching.

## Ca²⁺ channel mobility

To complete our findings, the dynamic behavior of the channels in the plasma membrane was directly visualized.

Repetitive imaging at a rate between 2 and 20 images/s was used to obtain a detailed picture of molecular movement in a biomembrane with a lateral resolution of <50 nm (Schmidt et al., 1996a). Analysis of image sequences of a typical length of 3–5 observations, limited by photobleaching, is used to construct the trajectories of individual signals on the cell membrane. All trajectories are confined to the cell perimeter (Fig. 5 *A*), which further confirms localization of the proteins in the plasma membrane. The lateral diffusion constant, $D_{lat}$, for each individual signal is calculated from the ratio of the mean-square displacement (msd) with the time-lag $t$, $D_{lat} = $ msd$/4t$, assuming normal diffusion behavior. That analysis yielded the histogram presented in Fig. 5 *B*. A Gamma distribution (Sonnleitner et al., 1999) with a mean of $D_{lat} = 0.15 \pm 0.05$ $\mu m^2$/s is used to describe the width of the histogram. That value falls well within the range of diffusion constants found for membrane proteins (Edidin, 1987). The diffusion behavior is further examined by a complementary analysis in which the time dependence of the mean-square displacement, averaged over all trajectories, was calculated (see Fig. 5 *B*, *inset*). We find that the msd is close to linear in time, at least up to the length scale of $\sqrt{0.5 \ \mu m^2} = 0.7$ $\mu m$. Hence, in that analysis any deviation from normal diffusion, which is expected for membrane proteins (Sonnleitner et al., 1999; Edidin, 1987; Simons and Ikonen, 1997), may occur on length scales $\gtrsim 1$ $\mu m$. Indeed, preliminary analysis according to anomalous subdiffusion behavior (Qian et al., 1991; Saxton, 1989) (msd $\propto t^{\alpha}$) yielded an exponent of $\alpha = 0.79 \pm 0.06$.

Fluorescence correlation spectroscopy (FCS) and fluorescence recovery after photobleaching experiments were used on the apical membrane of identical cells to confirm the single-molecule imaging results. In FCS an average of three eYFP-$\alpha_{1C,77}$ were present in the detection area of 0.32 $\mu m^2$, which corroborates the density found from the imaging experiments. The diffusion time obtained from the correlation experiments is $200 \pm 100$ ms (Fig. 5 *C*), yielding a lateral diffusion constant of $D_{lat} = 0.11 \pm 0.07$ $\mu m^2$/s. This value agrees with our findings of single-molecule microscopy (Fig. 5 *B*). It is noteworthy that on axially scanning through the cell, such long correlation times were only observable at the cell membrane (data not shown). The diffusion constant recorded at the membrane is a factor of 100 smaller than that obtained for cytosolic diffusion of nonfused eYFP, $D_{lat} = 20 \pm 5$ $\mu m^2$/s, and that for purified eYFP in solution, $D_{lat} = 21 \pm 5$ $\mu m^2$/s (Fig. 5 *C*, *inset*). Similar findings for membrane-bound and free molecules have been reported previously (Schwille et al., 1999; Swaminathan et al., 1997). Hence, we are confident to conclude that the L-type $Ca^{2+}$ channels observed were localized at the plasma membrane. Both the single-molecule imaging and FCS measurements further agree with fluorescence recovery after photobleaching measurements (data

not shown), yielding a diffusion constant of $D_{lat} = 0.13 \pm 0.05$ $\mu$m$^2$/s.

## DISCUSSION

To draw conclusions from the distribution of observed colocalized eYFP-$\alpha_{1C,77}$ molecules as displayed in Fig. 4 *C*, it must be compared with a theoretical model. For purely random colocalization within the resolution-limited area of the experiment (0.08 $\mu$m$^2$) a Poissonian distribution is predicted. The latter is characterized by the average number of detected eYFP-$\alpha_{1C,77}$ per resolution-limited area at the cell surface which was estimated from the number of identified signals in the experiments (see e.g., Fig. 3 *B*). The average density per resolution-limited area was ~0.24 eYFP-$\alpha_{1C,77}$ leading to the Poisson distribution indicated in Fig. 4 *C* (*blue open bars*). The predicted and the experimentally obtained distributions are significantly different. Hence, from our experiments we conclude that the L-type Ca$^{2+}$ channels form aggregates.

The conclusion is evidenced further by the corresponding electrophysiology experiments. Grouping of functional eYFP-$\alpha_{1C}$ channels rather than an even distribution in the plasma membrane sharply decreases the chance to detect channel activity in membrane patches. Clustering of the channel with a mean cluster size $M = 40$ will, at low plasmid transfection (Fig. 2 *C*), lead to the formation of <1 electrophysiological active patch per $\mu$m$^2$. This might explain our unsuccessful trials of patch-clamp recordings (1.7 $\mu$m$^2$ was the typical size of a membrane patch) at low plasmid concentration. At higher plasmid concentrations, clustering of functional L-type Ca$^{2+}$ channels has been reported in patch-clamp recordings (Kepplinger et al., 2000).

It seems surprising that clustering of the L-type Ca$^{2+}$ channel occurs in the expression system used, taking into account that HEK293 cells lack the excitation-contraction machinery of muscle cells which is believed to also govern the organization of L-type Ca$^{2+}$ channels (Hofmann et al., 1994; Flucher et al., 1993; Flucher and Franzini-Armstrong, 1996). It appears from our experiments that interaction of the channels with the ordered arrays of the Ca$^{2+}$-release channels inside the muscle cell (Flucher et al., 1993) seems to not be essentially needed for aggregation of L-type Ca$^{2+}$ channels. This result suggests that clustering is driven by self-aggregation of the protein.

In summary, we have demonstrated the viability of single-molecule fluorescence in vivo studies for quantitative elucidation of the dynamical embedding of L-type Ca$^{2+}$ channels in the plasma membrane as characterized by their lateral and rotational mobility and state of aggregation. With the swift rate of advances occurring in molecular biology along with the complex interactions of proteins taking place, we expect single-molecule microscopy to present a new perspective for research on molecular interactions, protein dynamics, and signaling pathways in living cells.

## REFERENCES

Catterall, W. A. 1995. Structure and function of voltage-gated ion channels. *Annu. Rev. Biochem.* 64:493–531.

Dickson, R. M., A. B. Cubitt, R. Y. Tsien, and W. E. Moerner. 1997. On/off blinking and switching behavior of single molecules of green fluorescent protein. *Nature.* 388:355–358.

Edidin, M. 1987. Rotational and lateral diffusion of membrane proteins and lipids: phenomena and function. *Curr. Top. Mem. Trans.* 29:91–127.

Edman, L., U. Mets, and R. Rigler. 1996. Conformational transitions monitored for single molecules in solution. *Proc. Natl. Acad. Sci. U.S.A.* 93:6710–6715.

Fabiato, A., and F. Fabiato. 1997. Calcium and cardiac excitation-contraction coupling. *Annu. Rev. Physiol.* 41:473–484.

Flucher, B. E., S. B. Andrews, S. Fleischer, A. R. Marks, A. Caswell, and J. A. Powell. 1993. Triad formation: organization and function of the sarcoplasmic reticulum calcium release channel and triadin in normal and dysgenic muscle in vitro. *J. Biol. Chem.* 270:1161–1174.

Flucher, B. E., and C. Franzini-Armstrong. 1996. Formation of junctions involved in excitation-contraction coupling in skeletal and cardiac muscle. *Proc. Natl. Acad. Sci. U.S.A.* 93:8101–8106.

Gao, T., A. J. Chien, and M. M. Hosey. 1999. Complexes of the $\alpha$1C and $\beta$ subunits generate the necessary signal for membrane targeting of class C L-type calcium channels *J. Biol. Chem.* 274:2137–2144.

Garcia-Parajo, M. F., G. M. Segers-Nolten, J. Veerman, J. Greve, and N. F. van Hulst. 2000. Real-time light-driven dynamics of the fluorescence emission in single green fluorescent protein molecules *Proc. Natl. Acad. Sci. U.S.A.* 97:7237–7242.

Gerster, U., B. Neuhuber, K. Groschner, J. Striessnig, and B. E. Flucher. 1999. Current modulation and membrane targeting of the calcium channel $\alpha$1C subunit are independent functions of the $\beta$ subunit. *J. Physiol.* 517:353–368.

Grabner, M., R. T. Dirksen, and K. G. Beam. 1998. Tagging with green fluorescent protein reveals a distinct subcellular distribution of L-type and non-L-type Ca$^{2+}$ channels expressed in dysgenic myotubes. *Proc. Natl. Acad. Sci. U.S.A.* 95:1903–1908.

Hamill, O. P., A. Marty, E. Neher, B. Sakmann, and F. J. Sigworth. 1981. Improved patch-clamp techniques for high-resolution current recording from cells and cell-free membrane patches. *Pflügers Arch.* 391:85–100.

Harms, G. S., M. Sonnleitner, G. J. Schütz, H. J. Gruber, and T. Schmidt. 1999. Single-molecule anisotropy imaging. *Biophys. J.* 77:2864–2870.

Harms, G. S., P. H. Lommerse, G. A. Blab, L. Cognet, and T. Schmidt. 2001. Autofluorescent proteins in single-molecule research. *Biophys. J.* 80:2396–2408.

Hinterdorfer, P., H. J. Gruber, J. Striessnig, H. Glossmann, and H. Schindler. 1997. Analysis of membrane protein self-association in lipid systems by fluorescence particle counting: application to the dihydropyridine receptor. *Biochemistry.* 36:4497–4504.

Hofmann, F., M. Biel, and V. Flockerzi. 1994. Molecular basis for Ca$^{2+}$ channel diversity. *Annu. Rev. Neurosci.* 17:399–418.

Ishii, Y., and T. Yanagida. 2000. Single-molecule detection in life sciences. *Single Mol.* 1:5–16.

Jia, Y. W., D. S. Talaga, W. L. Lau, H. S. Lu, W. F. DeGrado, and R. M. Hochstrasser. 1999. Folding dynamics of single GCN4 peptides by fluorescence resonant energy transfer confocal microscopy. *Chem. Phys.* 247:69–83.

Kepplinger, K. J., H. Kahr, G. Förstner, M. Sonnleitner, H. Schindler, T. Schmidt, K. Groschner, N. M. Soldatov, and C. Romanin. 2000. A sequence in the carboxy-terminus of the $\alpha_{1C}$ subunit important for targeting, conductance and open probability of L-type $Ca^{2+}$ channels *FEBS Lett.* 477:161–169.

Lu, H. P., L. Xun, and X. S. Xie. 1998. Single-molecule enzymatic dynamics. *Science.* 282:1877–1882.

Murphy, T. H., P. F. Worley, and J. M. Baraban. 1991. L-type voltage-sensitive calcium channels mediate synaptic activation of immediate early genes. *Neuron.* 7:625–635.

Neher E. 1992. Correction of liquid junction potentials in patch clamp experiments. *Methods Enzymol.* 207:123–131.

Nunoki, K., V. Florio, and W. A. Catterall. 1989. Activation of purified calcium channels by stoichiometric protein phosphorylation. *Proc. Natl. Acad. Sci. U.S.A.* 86:6816–6820.

Qian, H., M. P. Sheetz, and E. L. Elson. 1991. Single particle tracking. Analysis of diffusion and flow in two-dimensional systems. *Biophys. J.* 60:910–921.

Rios, E., and G. Brum. 1987. Involvement of dihydropyridine receptors in excitation-contraction coupling in skeletal muscle. *Nature.* 325: 717–720.

Saito, A., M. Inui, M. Radermacher, J. Frank, and S. Fleischer. 1988. Ultrastructure of the calcium release channel of sarcoplasmic reticulum *J. Cell Biol.* 107:211–219.

Sako, Y., S. Minoghchi, and T. Yanagida. 2000. Single-molecule imaging of EGFR signalling on the surface of living cells. *Nat. Cell Biol.* 2:168–172.

Sase, I., H. Miyata, S. Ishiwata, and K. Kinosita. 1997. Axial rotation of sliding actin filaments revealed by single-fluorophore imaging. *Proc. Natl. Acad. Sci. U.S.A.* 94:5646–5650.

Saxton, M. J. 1989. Lateral diffusion in an archipelago. Distance dependence of the diffusion coefficient. *Biophys. J.* 56:615–622.

Schmidt, T., G. J. Schütz, W. Baumgartner, H. J. Gruber, and H. Schindler. 1995. Characterization of photophysics and mobility of single molecules in a fluid lipid membrane. *J. Phys. Chem* 99:17662–17668.

Schmidt, T., G. J. Schütz, W. Baumgartner, H. J. Gruber, and H. Schindler. 1996a. Imaging of single molecule diffusion. *Proc. Natl. Acad. Sci. U.S.A.* 93:2926–2929.

Schmidt, T., G. J. Schütz, H. J. Gruber, and H. Schindler. 1996b. Local stoichiometries determined by counting individual molecules. *Anal. Chem.* 68:4397–4401.

Schütz, G. J., G. Kada, V. P. Pastushenko, and H. Schindler. 2000. Properties of lipid microdomains in a muscle cell membrane visualized by single molecule microscopy. *EMBO J.* 19:892–901.

Schwartz, L. M., E. W. McCleskey, and W. Almers. 1985. Dihydropyridine receptors in muscle are voltage-dependent but most are not functional calcium channels. *Nature.* 314:747–751.

Schwille, P., U. Haupts, S. Maiti, and W. W. Webb. 1999. Molecular dynamics in living cells observed by fluorescence correlation spectroscopy with one- and two-photon excitation. *Biophys. J.* 77:2251–2265.

Schwille, P., S. Kummer, A. A. Heikal, W. E. Moerner, and W. W. Webb. 2000. Fluorescence correlation spectroscopy reveals fast optical excitation-driven intramolecular dynamics of yellow fluorescent proteins. *Proc. Natl. Acad. Sci. U.S.A.* 97:151–156.

Simons, K., and E. Ikonen. 1997. Functional rafts in cell membranes. *Nature.* 387:569–572.

Sonnleitner, A., G. J. Schütz, and T. Schmidt. 1999. Free brownian motion of individual lipid molecules in biomembranes. *Biophys. J.* 77: 2638–2642.

Swaminathan, R., C. P. Hoang, and A. S. Verkman. 1997. Photobleaching recovery and anisotropy decay of green fluorescent protein GFP-S65T in solution and cells: cytoplasmic viscosity probed by green fluorescent protein translational and rotational diffusion. *Biophys. J.* 72:1900–1907.

Tsien, R. Y. 1998. The green fluorescent protein. *Annu. Rev. Biochem.* 67:509–544.

Van Oijen A. M., M. Ketelaars, J. Kohler, T. J. Aartsma, and J. Schmidt. 1999. Unraveling the electronic structure of individual photosynthetic pigment-protein complexes. Science. 285:400–402.

Weiss, S. 1999. Fluorescence spectroscopy of single biomolecules. *Science.* 283:1676–1683.

Widengren, J., and R. Rigler. 1998. Fluorescence correlation spectroscopy as a tool to investigate chemical reactions in solutions and on cell surfaces. *Cell Mol. Biol.* 44:857–879.

Widengren, J., B. Terry, and R. Rigler. 1999. Protonation kinetics of GFP and FITC investigated by FCS–aspects of the use of fluorescent indicators for measuring pH. *Chem. Phys.* 249:259–271.